



## ORIGINAL ARTICLE

# Evaluation of 10-minute post-injection $^{11}\text{C}$ -PiB PET and its correlation with $^{18}\text{F}$ -FDG PET in older adults who are cognitively healthy, mildly impaired, or with probable Alzheimer's disease

Camila de Godoi **Carneiro**,<sup>1,2</sup>  Daniele de Paula **Faria**,<sup>1,2</sup> Artur Martins **Coutinho**,<sup>1</sup> Carla Rachel **Ono**,<sup>1</sup> Fábio Luís de Souza **Duran**,<sup>3</sup> Naomi Antunes **da Costa**,<sup>3</sup> Alexandre Teles **Garcez**,<sup>1</sup> Paula Squarzoni **da Silveira**,<sup>3</sup> Orestes Vicente **Forlenza**,<sup>4</sup> Sonia Maria Dozzi **Brucki**,<sup>5</sup> Ricardo **Nitrini**,<sup>5</sup> Geraldo **Busatto Filho**,<sup>3</sup> Carlos Alberto **Buchpiguel**<sup>1</sup> 

<sup>1</sup>Laboratório de Medicina Nuclear (LIM 43), Departamento de Radiologia e Oncologia, Hospital das Clínicas, Faculdade de Medicina, Universidade de São Paulo (USP), São Paulo, SP, Brazil. <sup>2</sup>Centro de Investigação Translacional em Oncologia, Departamento de Radiologia e Oncologia, Hospital das Clínicas, Faculdade de Medicina, Universidade de São Paulo (USP), São Paulo, SP, Brazil. <sup>3</sup>Laboratório Neuro-Imagem em Psiquiatria (LIM 21), Departamento de Psiquiatria, Hospital das Clínicas, Faculdade de Medicina, USP, São Paulo, SP, Brazil. <sup>4</sup>Laboratório de Neurociências (LIM 27), Departamento de Psiquiatria, Hospital das Clínicas, Faculdade de Medicina, USP, São Paulo, SP, Brazil. <sup>5</sup>Departamento de Neurologia, Hospital das Clínicas, Faculdade de Medicina, USP, São Paulo, SP, Brazil.

**Objective:** Positron emission tomography (PET) allows in vivo evaluation of molecular targets in neurodegenerative diseases, such as Alzheimer's disease. Mild cognitive impairment is an intermediate stage between normal cognition and Alzheimer-type dementia. *In vivo* fibrillar amyloid-beta can be detected in PET using [ $^{11}\text{C}$ ]-labeled Pittsburgh compound B ( $^{11}\text{C}$ -PiB). In contrast, [ $^{18}\text{F}$ ] fluoro-2-deoxy-d-glucose ( $^{18}\text{F}$ -FDG) is a neurodegeneration biomarker used to evaluate cerebral glucose metabolism, indicating neuronal injury and synaptic dysfunction. In addition, early cerebral uptake of amyloid-PET tracers can determine regional cerebral blood flow. The present study compared early-phase  $^{11}\text{C}$ -PiB and  $^{18}\text{F}$ -FDG in older adults without cognitive impairment, amnesic mild cognitive impairment, and clinical diagnosis of probable Alzheimer's disease.

**Methods:** We selected 90 older adults, clinically classified as healthy controls, with amnesic mild cognitive impairment, or with probable Alzheimer's disease, who underwent an  $^{18}\text{F}$ -FDG PET, early-phase  $^{11}\text{C}$ -PiB PET and magnetic resonance imaging. All participants were also classified as amyloid-positive or -negative in late-phase  $^{11}\text{C}$ -PiB. The data were analyzed using statistical parametric mapping.

**Results:** We found that the probable Alzheimer's disease and amnesic mild cognitive impairment group had lower early-phase  $^{11}\text{C}$ -PiB uptake in limbic structures than  $^{18}\text{F}$ -FDG uptake. The images showed significant interactions between amyloid-beta status (negative or positive). However, early-phase  $^{11}\text{C}$ -PiB appears to provide different information from  $^{18}\text{F}$ -FDG about neurodegeneration.

**Conclusions:** Our study suggests that early-phase  $^{11}\text{C}$ -PiB uptake correlates with  $^{18}\text{F}$ -FDG, irrespective of the particular amyloid-beta status. In addition, we observed distinct regional distribution patterns between both biomarkers, reinforcing the need for more robust studies to investigate the real clinical value of early-phase amyloid-PET imaging.

**Keywords:** Positron emission tomography; amyloid; [ $^{11}\text{C}$ ]-labeled Pittsburgh compound B; perfusion; cerebral glucose metabolism; [ $^{18}\text{F}$ ]fluoro-2-deoxy-d-glucose; aging, neuroimaging

## Introduction

Alzheimer's disease (AD) is the most common form of dementia.<sup>1</sup> In addition to brain deposits of amyloid-beta ( $\text{A}\beta$ ) peptides, tau pathology and neuron loss are AD's pathological hallmarks. This degenerative disorder is

associated with early neurovascular dysfunction, contributing to disease pathogenesis.<sup>2</sup>

Mild cognitive impairment (MCI) is an intermediate stage between normal cognition and Alzheimer-type dementia.<sup>3,4</sup> Patients with MCI can be further categorized as amnesic (aMCI) or non-amnesic MCI.<sup>5</sup> The most

Correspondence: Carlos Alberto Buchpiguel, Universidade de São Paulo, Faculdade de Medicina da Universidade de São Paulo, Av. Dr. Arnaldo, 455, CEP 01255-090, São Paulo, SP, Brazil.  
E-mail: buch@usp.br

Submitted Nov 22 2021, accepted Mar 14 2022, Epub Aug 29 2022.

**How to cite this article:** Carneiro CG, Faria DP, Coutinho AM, Ono CR, Duran FL, da Costa NA, et al. Evaluation of 10-minute post-injection  $^{11}\text{C}$ -PiB PET and its correlation with  $^{18}\text{F}$ -FDG PET in older adults who are cognitively healthy, mildly impaired, or with probable Alzheimer's disease. Braz J Psychiatry. 2022;44:495-506. <http://doi.org/10.47626/1516-4446-2021-2374>

common form, aMCI, is associated with memory loss and increased risk of AD,<sup>6</sup> having a biomarker profile generally closer to AD than non-amnesic MCI.<sup>7</sup>

Neurodegenerative processes have been extensively investigated using positron emission tomography (PET) tracers such as Pittsburgh compound B (<sup>11</sup>C-PiB), which is used for *in vivo* detection of A $\beta$  plaques in the brain,<sup>8,9</sup> and, [<sup>18</sup>F]fluoro-2-deoxy-d-glucose (<sup>18</sup>F-FDG), which is used to estimate neuronal injury and synaptic dysfunction.<sup>10,11</sup>

The binding of <sup>11</sup>C-PiB to A $\beta$  in gray matter is specific and reversible, although white matter has a non-specific and non-saturable component, possibly due to its high lipid content, as well as a specific component due to affinity to the  $\beta$ -sheet structure present in the myelin.<sup>12</sup> Accordingly, when there is a pathological concentration of A $\beta$  plaques in the brain, PET images usually show variable levels of <sup>11</sup>C-PiB uptake in cortical tissue. Therefore, <sup>11</sup>C-PiB imaging has been validated as an amyloid biomarker for *in vivo* investigation of AD.<sup>8,13,14</sup>

However, in theory, <sup>11</sup>C-PiB PET imaging may provide two types of clinical information: cerebral perfusion when the images are acquired during the first few minutes after intravenous administration, and A $\beta$  plaque accumulation when the images are obtained later. Thus, it may serve as a dual biomarker.<sup>9,15-20</sup>

Early concentration of the A $\beta$  tracer <sup>11</sup>C-PiB in PET images is mainly determined by cerebral blood flow and, hypothetically, should be correlated with <sup>18</sup>F-FDG uptake, due to blood flow and metabolism coupling in the brain. Lipophilic tracers, such as <sup>11</sup>C-PiB, usually have a high first-pass influx rate ( $K_1$ ),<sup>21</sup> which correlates with the regional cerebral blood flow (rCBF) due to the high extraction fraction.<sup>22</sup>

Due to the phenomenon of flow-metabolism coupling, we would expect to find some degree of association between cerebral biodistribution of early <sup>11</sup>C-PiB (<sup>11</sup>C-ePiB) and <sup>18</sup>F-FDG PET.<sup>23-25</sup> Thus, <sup>11</sup>C-ePiB might serve as a surrogate for tissue perfusion and, indirectly, brain metabolism.<sup>26,27</sup>

Prior evidence suggests that vascular dysfunction can lead to neuronal dysfunction and neurodegeneration. Such disorders include accumulation of the A $\beta$  peptide in the brain and the vessel wall, respectively, reflecting synaptic loss due to neuronal injury by AD.<sup>2</sup> Some studies have shown that hypoperfusion and hypometabolism overlap in AD by detecting deficits in the posterior cingulate and posterior temporoparietal associative cortex.<sup>28-30</sup>

Different groups have investigated the potential value of initial phase amyloid study to reflect rCBF. Reports have compared rCBF estimates derived from summed <sup>11</sup>C-ePiB images and the washout allometric reference method for the  $R_1$  parameter in a standard reference tissue model. In general, these techniques are computationally demanding or only produce relative rCBF measures.<sup>31</sup>

Thus, considering the limited number of studies and their methodological differences, more research is clearly needed to investigate blood flow/metabolism coupling in specific brain regions using <sup>11</sup>C-ePiB and <sup>18</sup>F-FDG. This study aimed to explore the regional biodistribution differences between <sup>18</sup>F-FDG PET and <sup>11</sup>C-ePiB PET

measured in an early-phase interval of 0-10 minutes in older adults without cognitive impairment, with aMCI, or with a clinical diagnosis of probable AD.

## Methods

### Study population

Cognitively healthy volunteers and cognitively impaired subjects (with dementia compatible with AD or aMCI) were prospectively recruited at the Universidade de São Paulo's Hospital das Clínicas School of Medicine. This study was conducted in agreement with the 1964 Helsinki declaration and was approved by the institutional ethics committee (CAPPesq: n<sup>o</sup> 1.454.598). Written informed consent was obtained from all participants.

Ninety consecutive older adults were enrolled and divided into 3 main groups according to clinical and neuropsychological characteristics: 1) probable AD (n=27); 2) aMCI (n=39), and 3) cognitively healthy controls (n=24). All underwent full clinical evaluations, including structured interviews and a standardized comprehensive battery of neuropsychological tests.<sup>32-36</sup> A complete description of the patients can be found in Supplementary Text S1, available online only.

The final clinical diagnoses of either probable AD or aMCI were reached by a multidisciplinary consensus, considering the available clinical data gathered by neurologists, psychiatrists, and geriatricians. The patients met the 2011 National Institute of Neurological and Communicative Disorders and the Alzheimer's Disease and Related Disorders Association criteria for probable AD.<sup>37</sup> The severity of cognitive decline was accessed using the Blessed Scale<sup>38</sup> and the Portuguese version of the Mini-Mental State Examination (MMSE).<sup>39,40</sup>

The exclusion criteria were: age < 60 or > 90 years, history of diabetes mellitus, systemic disorders associated with cognitive decline, contraindications to performing magnetic resonance imaging (MRI), and brain lesions incidentally detected by MRI.

### Image acquisition

All subjects underwent brain MRI and PET with a 1-month interval between the scans (30.0 [standard deviation, SD = 10.3] days). On average, <sup>18</sup>F-FDG PET examinations were carried out 3.7 [SD = 0.7] days after acquiring the <sup>11</sup>C-ePiB PET data.

### T1-weighted MRI data acquisition

Anatomical MRI datasets were acquired using a Philips Achieva 3T scanner (software version 3.2.3/3.2.3.1; Philips Healthcare, Best, the Netherlands), at the hospital's radiology department, which was equipped with an 8-channel phased-array head coil according to the following protocol: T1-weighted datasets (3D) were acquired using the following parameters: TR 7 ms, TE 3.2 ms, flip angle 8 $\alpha$ , Sense 1.5, field of view 240  $\times$  240, matrix 240  $\times$  240, 180 slices of 1 mm each with no gap, yielding a voxel size of 1  $\times$  1  $\times$  1 mm.

### PET/CT data acquisition

Both the  $^{11}\text{C}$ -PiB and  $^{18}\text{F}$ -FDG tracers were produced on-site at the University's cyclotron facility (PETtrace™ 880, GE Healthcare), which is compliant with good manufacturing practices. The PET images were acquired using a Discovery 710 PET/computed tomography (CT) scanner (GE Healthcare, Milwaukee, WI, USA) at the Nuclear Medicine Division of the Department of Radiology and Oncology.

According to the institution's standard protocol, a brain CT scan was performed immediately prior to the PET scan using the same scanner, which was used to correct attenuation. CT was performed using a 70-100 mA range, 120 kV, and 0.5 s per rotation, with a slice thickness of 3.25 mm.

**$^{11}\text{C}$ -PiB PET.** Dynamic imaging commenced at injection and continued for 70 minutes. Summed images were created with data from 0 to 10 minutes (early-phase  $^{11}\text{C}$ -ePiB) and 40 to 70 minutes (late-phase  $^{11}\text{C}$ -PiB) post-administration (565 [SD = 124] MBq). Both the dynamic frames and the summed images were converted to standardized uptake value images. The early phase of the dynamic sequence (i.e., first 10 minutes) was used to characterize cerebral blood flow, consistent with previous studies,<sup>41,42</sup> while the latter phase was used to characterize amyloid burden. The static late-phase frame was reconstructed only for the clinical read-out of cerebral A $\beta$  pathology. The  $^{11}\text{C}$ -ePiB images were reconstructed using the following parameters: matrix 256 × 256 mm, iterative reconstruction method by ordered-subset expectation maximization, 24 subsets and 4 iterations, standardized processing algorithm (VUE Point HD) smoothed with Gaussian filter: full width at half maximum of 3 mm, and point spread function modeling (GE SHARP IR). The data were corrected for scattering, attenuation, dead time, and radioactive decay.

**$^{18}\text{F}$ -FDG PET.** Regarding  $^{18}\text{F}$ -FDG PET acquisition, participants fasted for a minimum of 6 hours. Blood glucose levels were measured and recorded immediately before  $^{18}\text{F}$ -FDG injection to ensure glucose levels below 200 mg/dL. The participants remained at rest without audiovisual stimuli and with their eyes open for at least 30 minutes after intravenous administration of  $^{18}\text{F}$ -FDG (212 [SD = 23] MBq). Data were acquired in static mode for 15 minutes with time-of-flight information and a 256 × 256 mm matrix. The data were reconstructed using the ordered-subset expectation maximization method (16 subsets and 4 iterations), with a standardized processing algorithm (VUE Point FX) smoothed with a Gaussian filter (full width at half maximum 3 mm) and point spread function modeling (GE SHARP IR). The data were corrected for scattering, attenuation, dead time, and radioactive decay.

### Data processing

The T1-weighted MRIs were pre-processed with the manual skull-stripping technique, and extracerebral structures (e.g., skull, fat, venous sinuses) were removed with MRICro™ software, version April 4, 2011

(<http://people.cas.sc.edu/rorden/micro/micro.html>) to improve robustness.<sup>43,44</sup>

The data were further analyzed using Statistical Parametric Mapping (SPM) software, version 12 (Wellcome Department of Imaging Neuroscience, Institute of Neurology, London, U.K.; <http://www.fil.ion.ucl.ac.uk/spm>), which was run on the MATLAB platform, version R2015a (The Mathworks Inc., USA; <http://www.mathworks.com/index>).

The PET images were co-registered to the T1-weighted MRI to voxel-based statistical analysis. All images were oriented manually to place the anterior commissure at the origin of the 3-dimensional Montreal Neurological Institute stereotaxic coordinate system. The T1-MRI datasets were then spatially normalized to standard Montreal Neurological Institute space using standard diffeomorphic anatomical registration through exponentiated lie algebra. The images were then parcellated into different tissue classes: gray matter, white matter, and non-brain voxels (such as the skull and cerebrospinal fluid), based on separate tissue probability maps for each tissue class using the segmentation approach processing pipeline in SPM.<sup>45</sup> The algorithm was used to generate a study-specific template, and the resulting flow fields were generated by diffeomorphic anatomical registration through exponentiated lie algebra. PET images were spatially normalized to MNI space using subject-specific transformation obtained from the Montreal Neurological Institute. The procedure was specifically designed for this study to obtain a more precise between-subject anatomical overlap. Finally, the images were spatially smoothed with a Gaussian kernel at a full-width half-maximum of 8 mm.

Proportional scaling to the global mean was used to minimize between-subject variability. After the spatial transformations, the total brain radioactive uptake measurement was automatically obtained by SPM, given the mean counts of all voxels included in each participant's PET volume, thus obtaining absolute quantitative value results. To ensure that the analysis only included voxels that mapped cerebral tissue, we selected a default threshold of 0.5 for the mean uptake.

To perform a voxel-wise correlation between  $^{11}\text{C}$ -ePiB and  $^{18}\text{F}$ -FDG, we used the MARSeille Boîte À Région d'Intérêt Toolbox (MarsBaR, version 0.44). Volumes of interest (VOI) were grouped using a weighted mean approach (incorporating the number of voxels per meta-VOI) into prefrontal, orbitofrontal, parietal, temporal, anterior, and posterior cingulate cortices, and the precuneus.<sup>46</sup> The values were defined as counts per voxel in each VOI, specifically in units of Bq/ml.

Datasets were evaluated individually through blinded visual inspection by two certified nuclear medicine physicians with more than five years of experience in the field. Further details can be found in Supplementary Text S2, available online only.

All subjects were classified individually in late-phase  $^{11}\text{C}$ -PiB PET as positive or negative based on visual interpretation assisted by the 3D-SSP semi-quantitative software (CortexID Suite® software, GE Healthcare), with a standardized uptake value ratio (SUVr) > 1.42 as the positivity criterion.

To quantify cortical A $\beta$  load, the SUVR of late-phase  $^{11}\text{C}$ -PiB were analyzed using PMOD 3.4 software (PMOD<sup>TM</sup> Technologies Ltda., Switzerland), as has been previously described.<sup>33</sup> In the PNEURO tool,  $^{11}\text{C}$ -PiB PET images were co-registered to a T1-weighted MRI of respective subjects, and brain parcellation was performed based on the HAMMERS atlas (83 regions) for generating different VOIs. Images were corrected for partial volume effect using the “VOI-based” correction method. After extracting the SUVR for all regions, we also generated a meta-VOI, combining values<sup>46</sup> normalized to the whole cerebellum.<sup>47</sup>

### Statistical analysis

Demographic data and clinical details were managed using the Research Electronic Data Capture method.<sup>48</sup> Comparisons of continuous demographic variables across the groups were performed using one-way analysis of variance with Bonferroni correction for multiple comparisons. Statistical analyses were performed in SPSS version 17 and GraphPad Prism version 6.0.

Differences across scans were estimated in a voxel-by-voxel analysis using SPM. In each comparison, two *t*-statistic maps corresponding to opposite contrasts (decrease or increase of perfusion/uptake) were generated. Significant differences between the regional distribution of  $^{11}\text{C}$ -ePiB and  $^{18}\text{F}$ -FDG were tested. In addition, unpaired *t*-tests were applied to examine the differences between each pair of groups (probable AD vs. control; probable AD vs. aMCI, and aMCI vs. control) for each method.

In addition to the between-group comparisons mentioned above, we ran partial linear correlation analyses between voxel-wise means in meta-VOI to further investigate A $\beta$  deposition relationships.

The findings in these exploratory analyses were considered significant if they survived correction for multiple comparisons with the family-wise error method ( $p_{\text{FWE}} \leq 0.05$ ), and clusters were reported as significant when they surpassed this level: only clusters with a voxel size  $> 10$  were considered. Moreover, these maps were inspected for clusters of differences (increase/decrease) using a significance threshold of  $p < 0.001$  (uncorrected for multiple comparisons) ( $Z = 3.09$ ). The anatomic location of each resulting cluster was determined using the Talairach and Tournoux Atlas coordinates,<sup>49</sup> converted from Montreal Neurological Institute space, and projected onto a template cortical surface.

## Results

### Sociodemographic description of the sample

The sociodemographic data and MMSE scores of the 90 participants are shown in Table 1. Groups were paired by age and sex. Regarding years of education, there were imbalances between healthy controls and the aMCI group ( $p = 0.027$ ) and between healthy controls and the probable AD group ( $p = 0.008$ ). Significant differences in MMSE score were found between the three groups ( $p < 0.05$ ), with the probable AD and aMCI groups performing worse than the control group, as expected.

Regarding late-phase  $^{11}\text{C}$ -PiB PET, there was a significant mean difference in SUVR between the groups (Table 2). The receiver operating characteristic curve for SUVR is shown in Figure S1, available as online-only supplementary material. Even though we could not obtain very high receiver operating characteristic curves to distinguish the clinical groups, it was clear that late phase  $^{11}\text{C}$ -PiB is a good test for differentiating healthy adults from those with probable AD (area under the curve (AUC): 0.775[SD = 0.06]).

### Differences in biodistribution between early-phase $^{11}\text{C}$ -PiB PET and glucose metabolism by $^{18}\text{F}$ -FDG PET

The first voxel-by-voxel analysis compared differences in regional cerebral uptake of  $^{11}\text{C}$ -ePiB and  $^{18}\text{F}$ -FDG within the groups, as shown in Figure 1.

In the healthy control group, large areas of decreased  $^{11}\text{C}$ -ePiB perfusion compared to  $^{18}\text{F}$ -FDG uptake were seen bilaterally in the prefrontal, orbitofrontal, posterior parietal and superior temporal regions. The aMCI group had similar results, although to a lesser extent. The probable AD group had significant reductions in  $^{11}\text{C}$ -ePiB in the same regions, although to a much lesser extent than the other two groups. On the other hand, SPM analysis showed several clusters of increased  $^{11}\text{C}$ -ePiB perfusion relative to  $^{18}\text{F}$ -FDG uptake, especially in the anterior pole of both temporal lobes, as well as in the brain stem (mainly in the pons), cerebellum, anterior cingulate, and thalamus. Higher blood flow was observed relative to glucose uptake in the temporo-amygdala regions in the control and aMCI groups, although with some differences. Brodmann areas of the difference between the groups are detailed in Tables S1 and S2, available as online-only supplementary material.

**Table 1** Demographic characteristics of the sample

	Control (n=24)	aMCI (n=39)	Probable AD (n=27)	p-value		
				Control vs. aMCI	Control vs. probable AD	aMCI vs. probable AD
Age in years (range)	71 $\pm$ 6.2 (60-81)	73 $\pm$ 5.9 (62-86)	74 $\pm$ 7.7 (60-87)	0.090	0.082	0.624
Gender (f/m)	19/5	29/10	18/9	0.670	0.328	0.505
Years of formal education	13 $\pm$ 5.0	10 $\pm$ 4.9	9 $\pm$ 5.3	0.027*	0.008*	0.373
MMSE scores	28 $\pm$ 1.4	26 $\pm$ 2.3	21 $\pm$ 3.8	0.001*	< 0.0001*	< 0.0001*

Groups based on clinical classification. Data presented as mean  $\pm$  standard deviation values (minimum-maximum). f = female; m = male; MMSE = Mini-mental state examination; aMCI = amnesic mild cognitive impairment; AD = Alzheimer's disease. The p-value corresponds to the results of one-way analysis of variance (ANOVA).

\* $p < 0.05$ .

**Table 2**  $^{11}\text{C}$ -PiB PET and  $^{18}\text{F}$ -FDG PET positivity and negativity among groups

Biomarker status	Groups (based on clinical classification)		
	Control (n=24)	aMCI (n=39)	Probable AD (n=27)
Late-phase $^{11}\text{C}$ -PiB PET (positive)	5 (21%)	14 (36%)	20 (74%)
Mean SUVr (range)	1.55 (1.30-1.76)	1.60 (1.16-2.12)	1.70 (1.26-2.01)
Late-phase $^{11}\text{C}$ -PiB PET (negative)	19 (79%)	25 (64%)	7 (26%)
Mean SUVr (range)	1.06 (0.94-1.22)	1.08 (0.99-1.21)	1.04 (0.95-1.17)
$^{18}\text{F}$ -FDG PET (N +)	1 (4%)	11 (28%)	20 (74%)
$^{18}\text{F}$ -FDG PET (N -)	23 (96%)	28 (72%)	7 (26%)

$^{11}\text{C}$ -PiB PET: SUVr (standard uptake value ratio) of  $^{11}\text{C}$ -PiB uptake using whole cerebellum as reference.

$^{18}\text{F}$ -FDG PET (N +): positive for AD neurodegeneration plus non-AD patterns; AD hypometabolism pattern typical/suggestive of AD pathology; non-AD hypometabolism pattern not typical of AD pathology; (N-): negative AD plus non-AD patterns.

$^{11}\text{C}$ -PiB = [ $^{11}\text{C}$ ]-labeled Pittsburgh compound-B;  $^{18}\text{F}$ -FDG = [ $^{18}\text{F}$ ]fluoro-2-deoxy-d-glucose; aMCI = amnesic mild cognitive impairment; AD = Alzheimer's disease; PET = positron emission tomography; SUVr = standardized uptake value ratio.

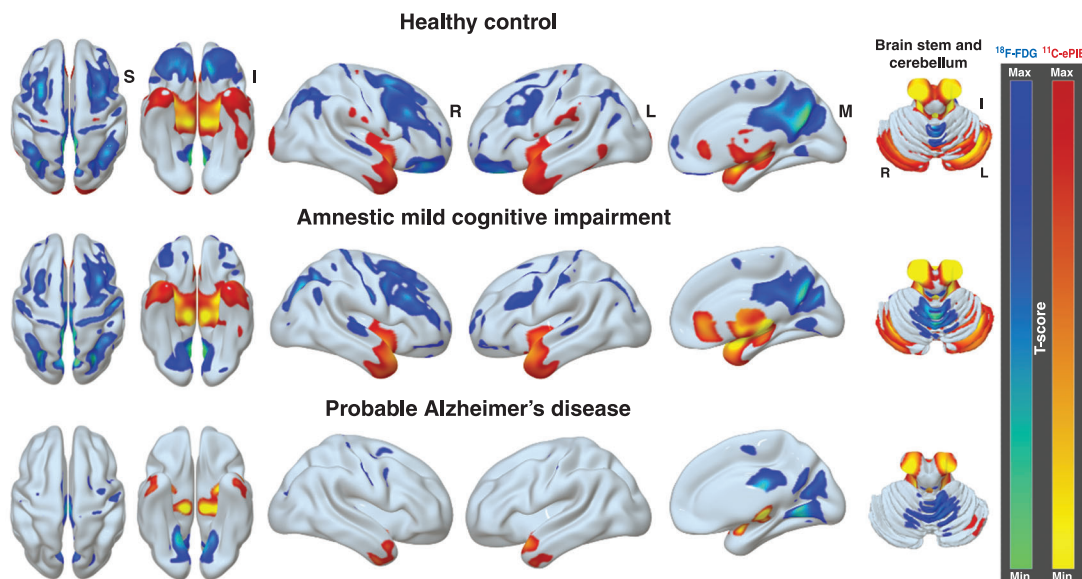


**Figure 1** Maximum-intensity projections of Statistical Parametric Mapping software  $t$ -maps showing biodistribution differences between the positron emission tomography tracers. Areas of decreased  $^{11}\text{C}$ -ePiB perfusion compared to  $^{18}\text{F}$ -FDG uptake in the groups appear in blue. Areas of increased  $^{11}\text{C}$ -ePiB perfusion compared to  $^{18}\text{F}$ -FDG uptake appear in red. The significance threshold was  $p < 0.05$ , corrected by the family wise error method.  $^{11}\text{C}$ -ePiB = early-phase [ $^{11}\text{C}$ ]-labeled Pittsburgh compound B;  $^{18}\text{F}$ -FDG = [ $^{18}\text{F}$ ]fluoro-2-deoxy-d-glucose; R = right; L = left; A = anterior; P = posterior; S = superior; I = inferior; M = medial.

When exploring voxel-wise correlations, we analyzed the relationship of  $\text{A}\beta$  status in the images (i.e.,  $^{11}\text{C}$ -ePiB vs.  $^{18}\text{F}$ -FDG). A moderate positive relationship was found across all regions (prefrontal/orbitofrontal, parietal, temporal, anterior/posterior cingulate and precuneus regions). Figure 2 shows differences in the correlated locations.

The healthy control group ( $\text{A}\beta$  PET-negative) had widespread and stronger correlations in multiple locations than  $\text{A}\beta$  PET-positive patients.  $\text{A}\beta$  PET-negatives in the aMCI group showed a mild correlation. Widespread and weaker correlations were found in multiple  $\text{A}\beta$  PET-negative patients than  $\text{A}\beta$  PET-positive patients in the prefrontal/orbitofrontal, parietal, temporal and precuneus regions. Finally, there was a moderate to a strong

relationship in prefrontal/orbitofrontal, anterior/posterior cingulate and precuneus regions between  $\text{A}\beta$  PET-positive and  $\text{A}\beta$  PET-negative patients in the AD group. No significant negative correlation was observed in the analysis.

#### *Differences between $^{11}\text{C}$ -ePiB and $^{18}\text{F}$ -FDG in regional brain uptake among probable AD or aMCI patients compared to healthy controls*

The differences between the probable AD and control groups are detailed in Table S3, available as online-only supplementary material, with years of education used as a covariate.



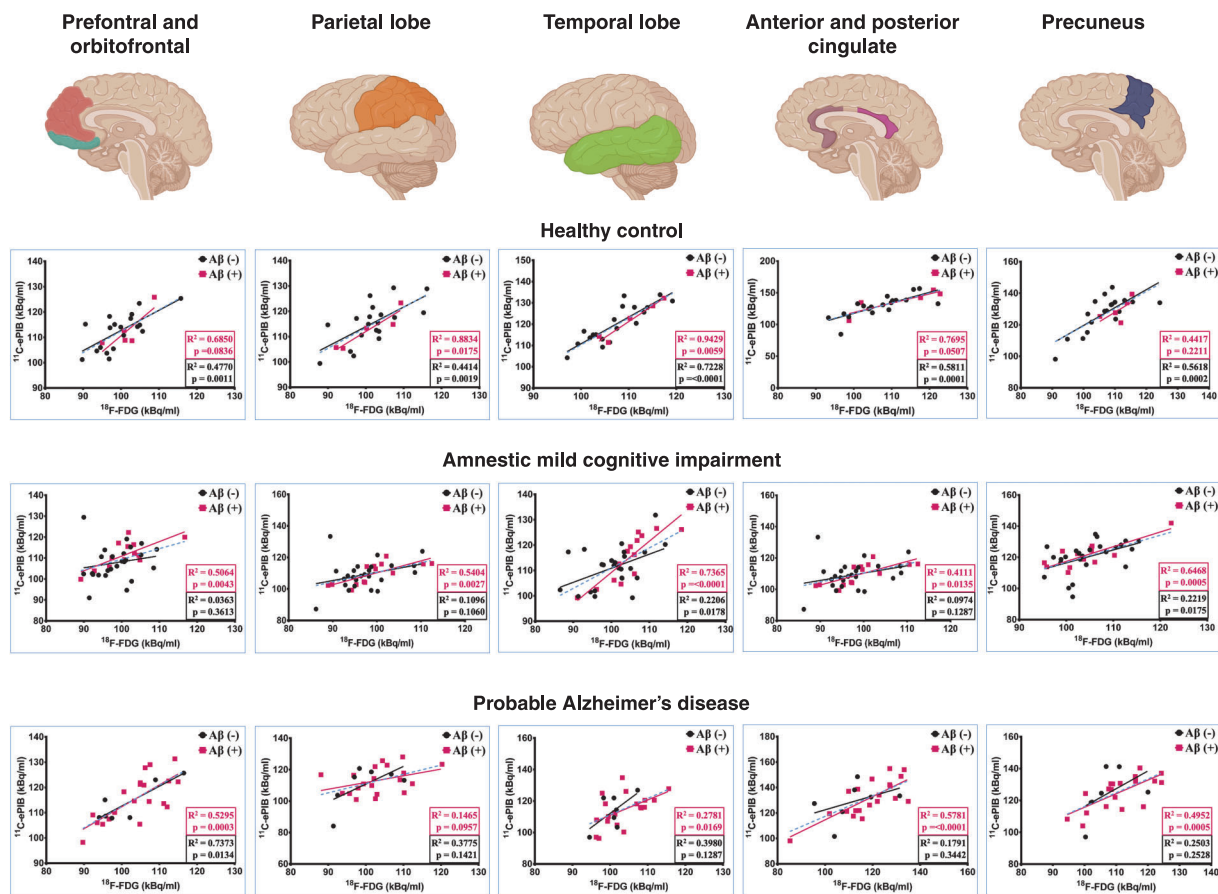


**Figure 2** Correlation across brain regions between early-phase [<sup>11</sup>C]-labeled Pittsburgh compound B (<sup>11</sup>C-ePiB) and [<sup>18</sup>F] fluoro-2-deoxy-d-glucose (<sup>18</sup>F-FDG) in the control, mild cognitive impairment, and probable Alzheimer's disease groups. The included areas are prefrontal, orbitofrontal, parietal, temporal, anterior and posterior cingulate, and the precuneus. Black circles and trendlines represent data from the <sup>11</sup>C-PiB-negative group, while pink circles and trendlines represent <sup>11</sup>C-PiB-positive group. Blue trendlines represent the combined groups (Aβ-negative and Aβ-positive). The authors created this illustration of meta-VOI in Biorender™ (<https://biorender.com/>).

The probable AD group had lower <sup>11</sup>C-ePiB perfusion than the control group in bilateral temporolimbic regions: parahippocampal gyrus (BA:36), hippocampus (BA:54), amygdala (BA:53) and the superior temporal gyrus (BA:38) (Figure 3A and B). The <sup>18</sup>F-FDG analysis revealed significantly more voxels of decreased <sup>18</sup>F-FDG uptake (lower metabolism) in the probable AD group than controls in the posterior cingulate cortex (BA:23) and precuneus (BA:31) (Figure 3C and D). A mild decrease in regional metabolic rate was also observed in the middle and inferior lateral temporal gyri (BA:39), but not in the mesial temporal and limbic structures.

We performed a secondary analysis of PET images, corrected partial volume effects, and checked gray matter volumes between groups, the results of which are shown in Supplementary Text S3, Figures S2 and S3, available as online-only supplementary material.

The comparison of the aMCI and healthy control groups is detailed in Table S4 (online only), with years of education used as a covariate. The aMCI group had

lower <sup>11</sup>C-ePiB perfusion than the control group in the hippocampus and parahippocampal gyrus (Figure S4A and B, available as online-only supplementary material), which was similar, but to a much lower degree, than the results of the probable AD group (Figure 3A and B). However, no differences were observed in <sup>18</sup>F-FDG uptake patterns between the aMCI and control groups.

#### *Analysis of <sup>11</sup>C-ePiB PET and <sup>18</sup>F-FDG PET, based amyloid-β biomarker status*

To determine whether amyloid burden status influenced the <sup>11</sup>C-ePiB results, we used a consensus diagnosis, assigning the diagnostic category based on conventional <sup>11</sup>C-PiB Aβ phase analysis (late-phase images 40 to 70 minutes after injection). Through this categorical method, each individual was classified as positive or negative <sup>11</sup>C-PiB PET, as previously described.<sup>33,34</sup> A total of 34 patients with aMCI and probable AD were subcategorized as <sup>11</sup>C-PiB-positive (aMCI, n=14 –

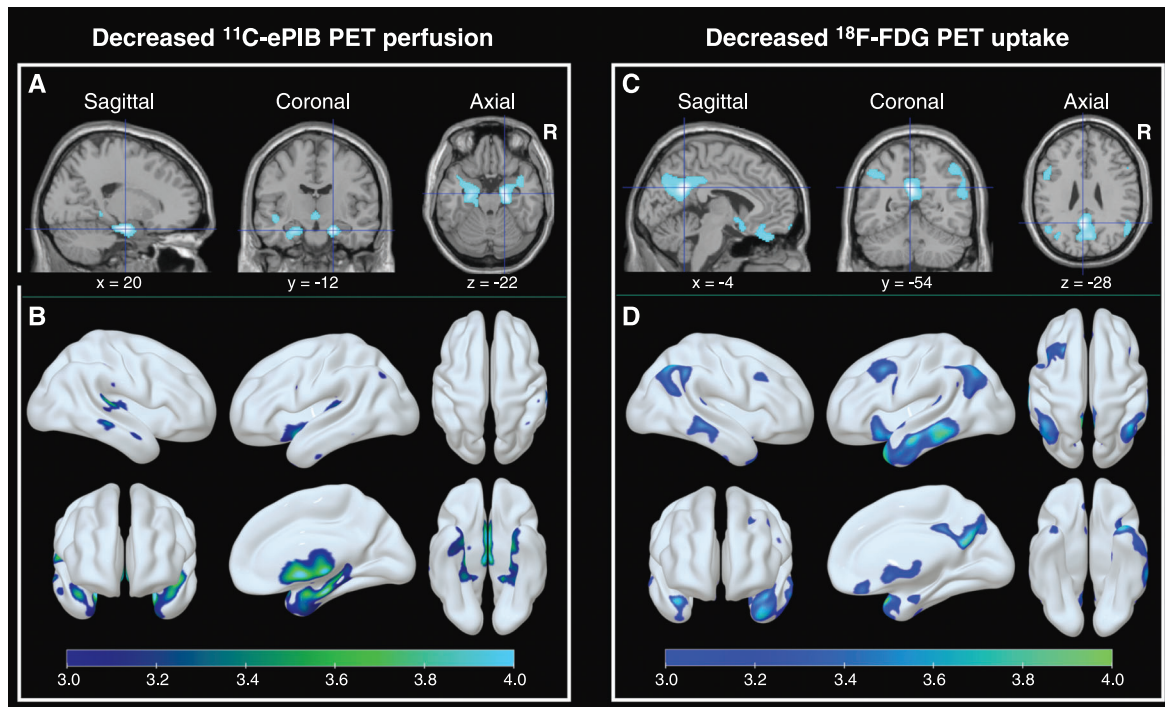


**Figure 3** Comparison between the probable Alzheimer's disease group ( $n=27$ ) and healthy controls ( $n=24$ ) with both positron emission tomography tracers. A) Areas of significantly decreased early-phase [ $^{11}\text{C}$ ]-labeled Pittsburgh compound B ( $^{11}\text{C}$ -ePiB) in the probable AD group are shown in blue, using volume-rendering images. B) Areas of decreased  $^{11}\text{C}$ -ePiB perfusion are shown in blue, with the main coordinates visualized in statistical parametric mapping template ch2. C) Areas of decreased [ $^{18}\text{F}$ ] fluoro-2-deoxy-d-glucose ( $^{18}\text{F}$ -FDG) uptake are shown in blue (volume-rendering visualization). D) Areas of decreased  $^{18}\text{F}$ -FDG uptake are shown in blue, with the main coordinates visualized in the statistical parametric mapping template ch2. The results were obtained through  $p < 0.05$  family-wise error method correction at the cluster level, with a previous height threshold of  $p < 0.001$ . The color scale indicates T-score values generated in statistical parametric mapping.

probable AD,  $n=20$ ), and 32 patients as  $^{11}\text{C}$ -PiB-negative (aMCI,  $n=25$  – probable AD,  $n=7$ ). We compared these groups with the healthy control group, which was  $^{11}\text{C}$ -PiB-negative ( $n=19$ ). See Figure 4.

#### $^{11}\text{C}$ -PiB-positive patients vs. healthy controls

$^{11}\text{C}$ -ePiB perfusion was significantly lower in the bilateral mesial temporal structures: hippocampus (BA:54; coordinates: -22, 2, -30 – cluster size ( $k_E$ ): 74,  $p_{\text{FWE}}$ : 0.001/BA:54; coordinates: 16, -38, -4 – cluster size ( $k_E$ ): 24,  $p_{\text{FWE}}$ : 0.016), large cluster extending into other regions: parahippocampal gyrus (BA:36), amygdala (BA:53), and the superior temporal pole (BA:38). Moreover,  $^{18}\text{F}$ -FDG PET glucose metabolism was decreased in the posterior cingulate cortex and precuneus regions (BA:23; coordinates: -40, 10, -18 – cluster size ( $k_E$ ): 401,  $p_{\text{FWE}}$ : 0.003; BA:31; coordinates: 0, -50, 34 – cluster size ( $k_E$ ): 12,  $p_{\text{FWE}}$ : 0.038).

#### $^{11}\text{C}$ -PiB-negative patients vs. healthy controls

Individuals categorized as cognitively abnormal (aMCI and AD) but with negative  $^{11}\text{C}$ -PiB PET results did not show an abnormal decrease of  $^{11}\text{C}$ -ePiB perfusion or  $^{18}\text{F}$ -FDG uptake, unlike the results of cognitively impaired patients with positive  $^{11}\text{C}$ -PiB PET results.

## Discussion

The present study's main finding was that although  $^{11}\text{C}$ -ePiB and  $^{18}\text{F}$ -FDG provide complimentary, significantly correlated data, they are not the same across all disease groups. This supports our first hypothesis that  $^{11}\text{C}$ -ePiB PET can serve as a robust indicator of neurodegeneration in individuals with probable AD and aMCI. These results support the value of  $^{11}\text{C}$ -PiB as a bi-functional imaging biomarker, highlighting significant differences with metabolic imaging findings typically seen in  $^{18}\text{F}$ -FDG.

We found significant relationships between the images, showing significant interactions between A $\beta$  status (negative or positive). Despite the visual similarities between the images and the biodistribution pattern of each PET tracer, the probable AD group had reduced perfusion in areas that commonly show atrophy in volumetric MRI and autopsy studies (i.e., medial temporal lobes),<sup>50</sup> but with preserved cerebral glucose metabolism.

These findings provide interesting insight into physiological and pathological brain aging. Although we selected a longer interval time frame for the perfusion phase of  $^{11}\text{C}$ -PiB (0 to 10 minutes) than other recent studies,<sup>31,51-54</sup> this did not seem to have compromised the comparison between these two molecular probes, since there were distribution differences among the three

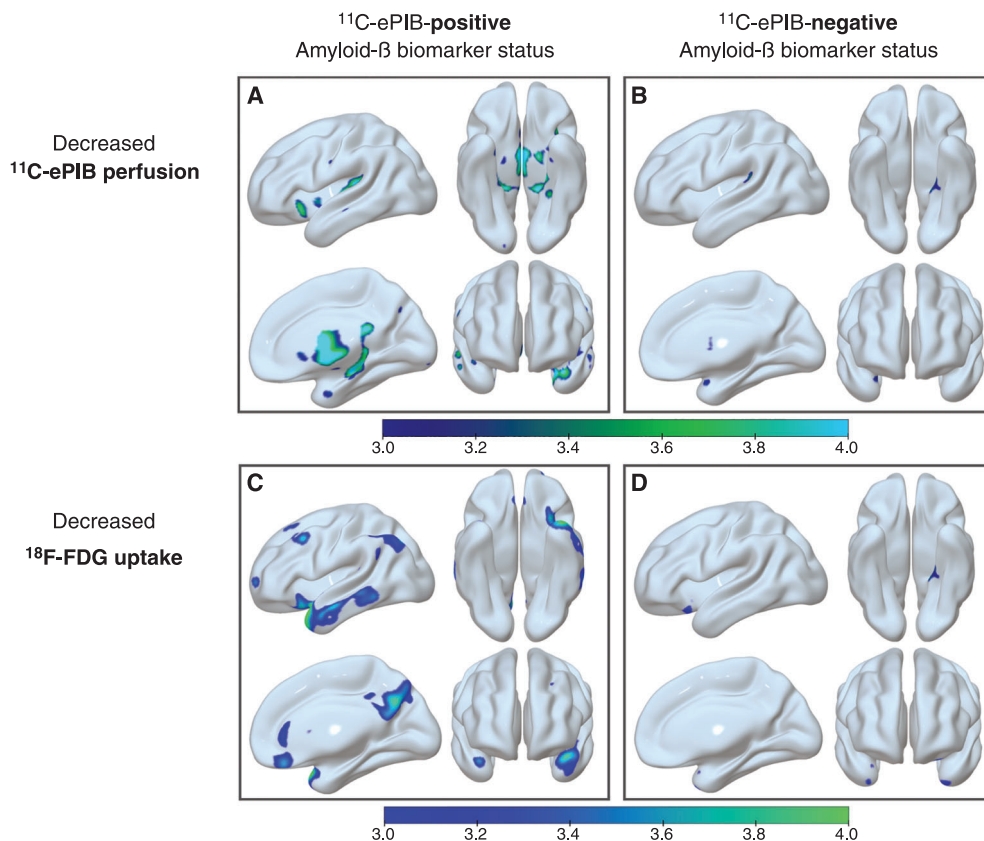


**Figure 4** Analysis of early-phase  $^{11}\text{C}$ -ePiB PET (0-10 minutes) and  $^{18}\text{F}$ -FDG-PET uptake, based on amyloid- $\beta$  biomarker status of  $^{11}\text{C}$ -PiB PET (40-70 minutes). We studied 34 patients  $^{11}\text{C}$ -PiB-positive (aMCI,  $n = 14$  - probable AD,  $n = 20$ ) and 32 patients  $^{11}\text{C}$ -PiB-negative (aMCI,  $n = 25$ ; probable Alzheimer's disease,  $n = 7$ ), vs. the healthy control group, which was  $^{11}\text{C}$ -PiB-negative ( $n=19$ ). A) Decreased  $^{11}\text{C}$ -ePiB perfusion in amyloid- $\beta$   $^{11}\text{C}$ -PiB-negative patients. B) Decreased  $^{11}\text{C}$ -ePiB perfusion in amyloid- $\beta$   $^{11}\text{C}$ -PiB-positive patients. C) Decreased  $^{18}\text{F}$ -FDG PET uptake in amyloid- $\beta$   $^{11}\text{C}$ -PiB-positive patients. D) Decreased  $^{18}\text{F}$ -FDG PET uptake in amyloid- $\beta$   $^{11}\text{C}$ -PiB-negative patients. The results were obtained using  $p < 0.05$  family-wise error correction on the cluster level, with a previous height threshold of  $p < 0.001$ . The bars indicate z scores, ranging from  $p = 10^{-3}$  (z score = 3.0) to  $p = 10^{-4}$  (z score = 4.0).  $^{11}\text{C}$ -ePiB = early-phase [ $^{11}\text{C}$ ]-labeled Pittsburgh compound B;  $^{18}\text{F}$ -FDG = [ $^{18}\text{F}$ ]fluoro-2-deoxy-d-glucose; aMCI: amnesic mild cognitive impairment group; PET = positron emission tomography.

groups. Moreover, if the longer interval used in this study could somehow account for higher tissue concentrations of  $^{11}\text{C}$ -PiB, it would be hard to explain how probable AD and aMCI patients had lower uptake of  $^{11}\text{C}$ -ePiB in limbic structures than  $^{18}\text{F}$ -FDG. These regions are known to show increased fibrillar A $\beta$  burden in AD. A $\beta$  pathology progression seems to begin in the neocortex with a few diffuse plaques and then progresses to the hippocampus, entorhinal cortex, cingulate cortex, and amygdala.<sup>55</sup>

In the present study, comparisons across groups were conducted using both radiopharmaceuticals independently to determine whether different tracers show distinct signs of neurodegeneration in each phase of the AD spectrum. Patients with probable AD had lower  $^{18}\text{F}$ -FDG uptake than controls mainly in the posterior cingulate cortex (PCC) and default mode network nodes, while decreased  $^{11}\text{C}$ -ePiB perfusion was found in the superior temporal gyrus and limbic mesial temporal lobe areas, indicating distinct but complementary regions with reduced metabolism and perfusion.

Furthermore, compared to the aMCI and control groups, the probable AD group had relatively lower uptake of  $^{18}\text{F}$ -FDG than  $^{11}\text{C}$ -ePiB, especially in the PCC and the temporoparietal regions. This may suggest that uptake deficits in the posterior association cortex and PCC are more easily identified with  $^{18}\text{F}$ -FDG than with the perfusion phase of  $^{11}\text{C}$ -PiB. This finding was also replicated in the analyses, using the same biomarker between groups (Figures 1 and 3).

$^{18}\text{F}$ -FDG uptake seems closely related to glial activity in neuronal synapses.<sup>56</sup> The lower relative concentration of  $^{18}\text{F}$ -FDG in the cerebellum compared to perfusion may be associated with the different density of glial cells in relation to neurons between the cerebral and cerebellar cortices. In primates, there is a lower glia/neuron rate in the cerebellum than in the cerebral cortex,<sup>57</sup> probably explaining the lower relative  $^{18}\text{F}$ -FDG uptake in this area. The same phenomenon may occur in other human brain areas, which would at least partially explain uncoupling in regional blood-flow/metabolism.



In fact, given the large between-subject variability in the topography of the disease, understanding factors that explain variability in level and change over time in  $^{11}\text{C}$ -PiB retention may help differentiate between normal aging and cognitive impairment. CBF alterations and A $\beta$  accumulation have been independently linked to cognitive deficits in older adults at risk for dementia. Less is known about how CBF and A $\beta$  interact to affect cognition in cognitively normal older adults. Although regional decreases in CBF are interpreted as reflecting decreased brain function, increases in perfusion in the context of preclinical AD, particularly when cognitive performance is maintained or improved, has often been considered a compensatory response to an incipient pathological process.<sup>58,59</sup>

Of note, the main discriminatory factor between the groups was clinical diagnosis. We also found this to remain consistent when re-analyzed based on A $\beta$  biomarker status. There was a close relationship between decreased  $^{11}\text{C}$ -ePiB perfusion and  $^{18}\text{F}$ -FDG uptake only in the A $\beta$   $^{11}\text{C}$ -PiB-positive group, but not in the A $\beta$   $^{11}\text{C}$ -PiB-negative group, which suggests a possible interaction between A $\beta$  deposition and reduced rCBF. This led us to infer that non-significant A $\beta$  uptake in brain tissue might have impaired our  $^{11}\text{C}$ -ePiB results, since the findings of reduced “perfusion” remained when compared to the  $^{11}\text{C}$ -PiB-negative group, which did not have reduced  $^{11}\text{C}$ -ePiB perfusion in any brain region. Probable AD was strongly associated with amyloid positivity. There was a strong association between amyloid positivity and positive neurodegeneration patterns in the probable AD and aMCI groups, with the majority of amyloid-positive patients being classified as N+ in those two groups, particularly in those with an AD-hypometabolic pattern.

Nevertheless, we found decreased metabolism in the association cortex and posterior cingulate gyrus in our sample of probable AD patients, as well as in the  $^{11}\text{C}$ -PiB-positive group (probable AD and aMCI). Still, no deficit in “perfusion” (according to  $^{11}\text{C}$ -ePiB concentration) was seen in the same groups, again raising the question whether uncoupling would be more prevalent in the limbic structures than in the association cortex or PCC.

Our study’s findings strengthen the hypothesis that  $^{18}\text{F}$ -FDG PET reflects activity in the default mode network, whereas  $^{11}\text{C}$ -ePiB PET probably does not. In 2014, Leech and Sharp showed that functional connectivity within the default mode network is reduced at AD onset, a change that mainly affects the connection between the PCC and the hippocampus. Altered patterns of functional connectivity of the PCC also reflect the genetic status of apolipoprotein E, a risk factor for AD.<sup>60</sup> Reduced metabolism in the PCC is also associated with A $\beta$  deposition and brain atrophy in a spatial distribution that strikingly reflects the nodes of the default mode network.<sup>61</sup>

These findings were more pronounced in probable AD than in aMCI patients, as would be expected according to the theory of longitudinal progression. It raises the question of whether neurovascular uncoupling is related to upregulation of metabolism in areas that have suffered from continuous neuronal loss and brain atrophy, as is usually seen in patients with AD. Depending on the status

of the compensatory mechanism, the glucose metabolic rate in patients with AD may initially increase and then subsequently decrease,<sup>62</sup> which could explain the findings of reduced perfusion in mesial temporal structures (in  $^{11}\text{C}$ -ePiB images) but no changes in  $^{18}\text{F}$ -FDG uptake in the same regions.

Several authors have reported<sup>28,29,63,64</sup> that decreased metabolism in the PCC is an early sign of AD and may result in a decline of cognitive function over time. While hypometabolism in the temporoparietal and PCC is a reliable predictor of progression to AD, this pattern has also been reported in patients with aMCI. However, in our sample of aMCI patients, no differences were observed in regional perfusion/uptake of both tracers compared to healthy controls. As shown in Figure 3, it was intriguing to find more significantly reduced perfusion of  $^{11}\text{C}$ -ePiB in the mesial temporal lobes rather than a greater reduction of glucose metabolism in the PCC in patients with probable AD. Again, this may suggest that the 0-to-10-minute interval chosen to represent the earliest perfusion status of  $^{11}\text{C}$ -PiB was unaffected by cortical retention ratios of A $\beta$  deposition.

The main differences in regional uptake between  $^{18}\text{F}$ -FDG PET and  $^{11}\text{C}$ -ePiB PET images were observed in subcortical and white matter regions (lower metabolism), whereas  $^{11}\text{C}$ -ePiB PET showed lower cortical perfusion than  $^{18}\text{F}$ -FDG PET in several large clusters. In all groups, we found dissociations in specific regions, such as the corticospinal tract, cerebellum, and thalamus, which had higher relative perfusion of  $^{11}\text{C}$ -ePiB than  $^{18}\text{F}$ -FDG uptake.

The dissociation patterns may reflect the differences between tracer properties and biodistribution patterns. While the basis for increased  $^{11}\text{C}$ -PiB uptake in white matter is unknown, it is associated with higher lipid composition, slower blood perfusion rate and, hence, slower delivery of the radioligand and clearance rates than gray matter.<sup>14,65</sup> White matter uptake is commonly observed in amyloid-PET studies using different A $\beta$  tracers, independent of cortical A $\beta$  deposition, both in cognitively impaired and unimpaired individuals.<sup>66</sup> Furthermore, the finding that A $\beta$  has different associations with rCBF and volume is consistent with the view that functional and synaptic loss is an early event in Alzheimer’s disease, leading to reduced rCBF prior to gray matter loss.<sup>67</sup>

A recent article<sup>68</sup> suggests that regional measures of  $^{11}\text{C}$ -PiB, particularly the relative delivery parameter R1 computed from dynamic  $^{11}\text{C}$ -PiB, can be a valid surrogate index of rCBF. This dual-imaging property may obviate additional  $^{18}\text{F}$ -FDG PET scanning, thereby reducing patient investigation time, radiation exposure, and, especially, cost.<sup>68</sup> Moreover, other earlier  $^{11}\text{C}$ -PiB times that better corresponded with the influx of the tracer into the brain have resulted in high-quality rCBF images comparable to those obtained by  $^{18}\text{F}$ -FDG SUVr.<sup>53,54</sup>

Another exciting possibility is additional comparative clinical studies with arterial spin labeling perfusion MRI, which uses magnetically labeled arterial blood water as a tracer and yields very similar image patterns and comparable diagnostic accuracy to  $^{18}\text{F}$ -FDG PET.

Significant positive correlations between CBF and cognition have been detected using arterial spin labeling perfusion MRI. These correlations may support the idea that rCBF could be a biomarker of neural changes due to cognitive decline.<sup>69</sup>

A previous study<sup>26</sup> found that an optimal relative quantitative analysis of early-phase <sup>18</sup>F-florbetaben acquisitions arises from global mean normalization, with little effect from the particular time frame (0-5 or 0-10 min). The <sup>18</sup>F-florbetaben uptake in the first ten minutes post-injection yields a perfusion-like image, evidently serving as a valid surrogate marker for synaptic and metabolic dysfunction, which would otherwise be revealed in a separate <sup>18</sup>F-FDG PET scan.

The potential advantage of using different temporal phases of <sup>11</sup>C-ePiB concentration in brain tissue to provide distinct functional information has been investigated previously with intriguing results. Discrepancies between our findings and those of other studies may be attributable to a series of factors, including selection criteria, demographics, the inclusion of other dementia syndromes, disease severity, etc. In an attempt to determine the optimal time frame for representing perfusion through <sup>11</sup>C-ePiB data, a previous study<sup>15</sup> found a high correlation between perfusion, measured in minutes 1-8 of an <sup>11</sup>C-PiB PET scan, and metabolism, measured by <sup>18</sup>F-FDG PET, although it enrolled a relatively small cohort of subjects who had a variety of neurodegenerative disorders. Of note, no relationship was found between quantitative measures of a 1-8 minute interval (no distinction between <sup>11</sup>C-PiB-positive and <sup>11</sup>C-PiB-negative groups).<sup>53,54</sup> Furthermore, we found other earlier <sup>11</sup>C-PiB times that better corresponded with tracer influx and resulted in high-quality rCBF images comparable with those obtained by <sup>18</sup>F-FDG SUVR (standardized uptake value ratios).<sup>53,54</sup> Gietl et al. found no associations between <sup>11</sup>C-ePiB frames and A $\beta$  positivity. Another study<sup>16</sup> that included AD and MCI patients reported lower values of <sup>11</sup>C-ePiB in the <sup>11</sup>C-PiB-positive group than the <sup>11</sup>C-PiB-negative group in the posterior cingulate cortex and parietal cortex, whereas there were widespread differences in <sup>18</sup>F-FDG in cortical and subcortical gray matter.

Our arbitrary determination of a 0-10-minute interval for <sup>11</sup>C-ePiB images, which was considered to represent the cerebral blood flow/perfusion distribution pattern of this particular tracer, could be mentioned as one limiting factor. Most published data so far has only included images acquired up to 8 minutes after injection. However, it would be hard to say that adding 2 more minutes (considering 10 minutes as the threshold) might have compromised the main concept and hypotheses of this study. Theoretically, adding further statistics to the summed images could have resulted in a more adequate visual and quantitative analysis.

In the present study, we did not validate the concept of <sup>11</sup>C-ePiB perfusion using other methodologies or imaging biomarkers, such as <sup>15</sup>O-H<sub>2</sub>O PET or even brain perfusion SPECT, to prove that we were observing the same physiological phenomena. We assumed that the early phases could represent blood perfusion through

the volume distribution of <sup>11</sup>C-PiB in brain tissue, without significant attachment to A $\beta$  plaques.

One potential benefit of using a single biomarker imaging study to provide dual-function data is that it would reduce overall patient investigation time, radiation exposure, and further costs. However, cost-effectiveness analysis should determine whether excluding <sup>18</sup>F-FDG PET and adding early and late phase amyloid imaging would reduce the overall cost without compromising accuracy.

In conclusion, our study suggests that images obtained from 0 to 10 minutes during the early phase of <sup>11</sup>C-PiB uptake correlate with <sup>18</sup>F-FDG, irrespective of amyloid status. However, distinct regional distribution patterns between both biomarkers were seen in individuals with probable AD and aMCI, reinforcing the need for more robust studies to investigate the real clinical value of early-phase amyloid-PET imaging.

### Acknowledgements

This study was supported by the São Paulo Research Foundation (FAPESP: number 2012/50329-6). The authors would like to thank all of our patients and their caregivers for making this study possible. The Departments of Neurology and Psychiatry at the University of São Paulo Hospital das Clínicas School of Medicine. Special thanks to Douglas dos Santos Picolo for support during neuroimaging data collection.

### Disclosure

The authors report no conflicts of interest.

### Reference

- 1 Querfurth HW, LaFerla FM. Alzheimer's disease. *New Engl J Med*. 2010;362:329-44.
- 2 Kisler K, Nelson AR, Montagne A, Zlokovic BV. Cerebral blood flow regulation and neurovascular dysfunction in Alzheimer disease. *Nat Rev Neurosci*. 2017;18:419-34.
- 3 Petersen RC, Doody R, Kurz A, Mohs RC, Morris JC, Rabins PV, et al. Current concepts in mild cognitive impairment. *Arch Neurol*. 2001;58:1985-92.
- 4 Petersen RC, Smith GE, Waring SC, Ivnick RJ, Tangalos EG, Kokmen E. Mild cognitive impairment: clinical characterization and outcome. *Arch Neurol*. 1999;56:303-8.
- 5 Csukly G, Sirály E, Fodor Z, Horváth A, Salacz P, Hidas Z, et al. The differentiation of amnesic type MCI from the non-amnesic types by structural MRI. *Front Aging Neurosci*. 2016;8:52.
- 6 Kaduszkiewicz H, Eisele M, Wiese B, Prokein J, Luppá M, Luck T, et al. Prognosis of Mild cognitive impairment in general practice: results of the German ageCoDe study. *Ann Fam Med*. 2014;12:158-65.
- 7 Coutinho AMN, Porto FHG, Duran FLS, Prando S, Ono CR, Feitosa EAAF, et al. Brain metabolism and cerebrospinal fluid biomarkers profile of non-amnesic mild cognitive impairment in comparison to amnesic mild cognitive impairment and normal older subjects. *Alzheimer's Res Ther*. 2015;7:58.
- 8 Klunk WE, Engler H, Nordberg A, Wang Y, Blomqvist G, Holt DP, et al. Imaging brain amyloid in Alzheimer's disease with Pittsburgh compound-B. *Ann Neurol*. 2004;55:306-19.
- 9 Meyer PT, Hellwig S, Amtage F, Rottenburger C, Sahn U, Reuland P, et al. Dual-biomarker imaging of regional cerebral amyloid load and neuronal activity in dementia with PET and <sup>11</sup>C-labeled Pittsburgh compound B. *J Nucl Med*. 2011;52:393-400.

- 10 Kato T, Inui Y, Nakamura A, Ito K. Brain fluorodeoxyglucose (FDG) PET in dementia. *Ageing Res Rev.* 2016;30:73-84.
- 11 Tripathi M, Tripathi M, Sharma R, Jaimini A, Md'souza M, Saw S, et al. Functional neuroimaging using F-18 FDG PET/CT in amnesic mild cognitive impairment: a preliminary study. *Indian J Nucl Medicine.* 2013;28:129-33.
- 12 Fodero-Tavoletti MT, Rowe CC, McLean CA, Leone L, Li QX, Masters CL, et al. Characterization of PiB binding to white matter in Alzheimer disease and other dementias. *J Nucl Med.* 2009;50:198-204.
- 13 Cohen AD, Klunk WE. Early detection of Alzheimer's disease using PiB and FDG PET. *Neurobiol Dis.* 2014;72 Pt A:117-22.
- 14 Veronese M, Bodini B, Garcia-Lorenzo D, Battaglini M, Bongarzone S, Comtat C, et al. Quantification of [(11C)PiB] PET for imaging myelin in the human brain: a test-retest reproducibility study in high-resolution research tomography. *J Cereb Blood Flow Metab.* 2015; 35:1771-82.
- 15 Rostomian AH, Madison C, Rabinovici GD, Jagust WJ. Early <sup>11</sup>C-PiB frames and <sup>18</sup>F-FDG PET measures are comparable: a study validated in a cohort of AD and FTDL patients. *J Nucl Med.* 2011;52:173-9.
- 16 Forsberg A, Engler H, Blomquist G, Långström B, Nordberg A. The use of PiB-PET as a dual pathological and functional biomarker in AD. *Biochim Biophys Acta.* 2012;1822:380-5.
- 17 Fu L, Liu L, Zhang J, Xu B, Fan Y, Tian J. Comparison of dual-biomarker PiB-PET and dual-tracer PET in AD diagnosis. *Eur Radiol.* 2014;24:2800-9.
- 18 Fu L, Liu L, Zhang J, Xu B, Fan Y, Tian J. Brain network alterations in Alzheimer's disease identified by early-phase PiB-PET. *Contrast Media Mol Imaging.* 2018 Jan 8; 2018:6830105. doi: 10.1155/2018/6830105. eCollection 2018.
- 19 Rodriguez-Vieitez E, Carter SF, Chiotis K, Saint-Aubert L, Leuzy A, Schöll M, et al. Comparison of early-phase <sup>11</sup>C-deuterium-l-deprenyl and <sup>11</sup>C-Pittsburgh compound B PET for assessing brain perfusion in Alzheimer disease. *J Nucl Med.* 2016;57:1071-7.
- 20 Tiepolt S, Hesse S, Patt M, Luthardt J, Schroeter ML, Hoffmann KT, et al. Early [<sup>18</sup>F]florbetaben and [<sup>11</sup>C]PiB PET images are a surrogate biomarker of neuronal injury in Alzheimer's disease. *Eur J Nucl Med Mol Imaging.* 2016;43:1700-9.
- 21 Dishino DD, Welch MJ, Kilbourn MR, Raichle ME. Relationship between lipophilicity and brain extraction of C-11-labeled radiopharmaceuticals. *J Nucl Med.* 1983;24:1030-8.
- 22 Blomquist G, Engler H, Nordberg A, Ringheim A, Wall A, Forsberg A, et al. Unidirectional influx and net accumulation of PiB. *Open Neuroimaging J.* 2008;2:114-25.
- 23 Silverman DHS. Brain <sup>18</sup>F-FDG PET in the diagnosis of neurodegenerative dementias: comparison with perfusion SPECT and with clinical evaluations lacking nuclear imaging. *J Nucl Med.* 2004;45: 594-607.
- 24 Nihashi T, Yatsuya H, Hayasaka K, Kato R, Kawatsu S, Arahata Y, et al. Direct comparison study between FDG-PET and IMP-SPECT for diagnosing Alzheimer's disease using 3D-SSP analysis in the same patients. *Radiat Med.* 2007;25:255-62.
- 25 Herholz K. Perfusion SPECT and FDG-PET. *Int Psychogeriatr.* 2011;23. Suppl 2: S25-31.
- 26 Daerr S, Brendel M, Zach C, Mille E, Schilling D, Zacherl MJ, et al. Evaluation of early-phase [<sup>18</sup>F]florbetaben PET acquisition in clinical routine cases. *Neuroimage Clin.* 2016;14:77-86.
- 27 Joseph-Mathurin N, Su Y, Blazey TM, Jasielc M, Vlassenko A, Friedrichsen K, et al. Utility of perfusion PET measures to assess neuronal injury in Alzheimer's disease. *Alzheimers Dement (Amst).* 2018;10:669-77.
- 28 Johnson KA, Moran EK, Becker JA, Blacker D, Fischman AJ, Albert MS. Single photon emission computed tomography perfusion differences in mild cognitive impairment. *J Neurology Neurosurg Psychiatry.* 2007;78:240-7.
- 29 Minoshima S, Giordani B, Berent S, Frey KA, Foster NL, Kuhl DE. Metabolic reduction in the posterior cingulate cortex in very early Alzheimer's disease. *Ann Neurol.* 1997;42:85-94.
- 30 Edison P, Archer HA, Hinz R, Hammers A, Pavese N, Tai YF, et al. Amyloid, hypometabolism, and cognition in Alzheimer disease: an [<sup>11</sup>C]PiB and [<sup>18</sup>F]FDG PET study. *Neurology.* 2007;68:501-8.
- 31 Ponto LLB, Moser DJ, Menda Y, Harlynn EL, DeVries SD, Oleson JJ, et al. Early phase PiB-PET as a surrogate for global and regional cerebral blood flow measures. *J Neuroimaging.* 2019;29:85-96.
- 32 Busatto GF, de Gobbi Porto FH, Faria DP, Squarzoni P, Coutinho AM, Garcez AT, et al. In vivo imaging evidence of poor cognitive resilience to Alzheimer's disease pathology in subjects with very low cognitive reserve from a low-middle income environment. *Alzheimers Dement (Amst).* 2020;12:e12122.
- 33 Busatto GF, Duran FLS, Squarzoni P, Coutinho AMN, Rosa PGP, Torralbo L, et al. Hippocampal subregional volume changes in elders classified using positron emission tomography-based Alzheimer's biomarkers of  $\beta$ -amyloid deposition and neurodegeneration. *J Neurosci Res.* 2021;99:481-501.
- 34 Coutinho AM, Busatto GF, de Gobbi Porto FH, Faria DP, Ono CR, Garcez AT, et al. Brain PET amyloid and neurodegeneration biomarkers in the context of the 2018 NIA-AA research framework: an individual approach exploring clinical-biomarker mismatches and sociodemographic parameters. *Eur J Nucl Med Mol Imaging.* 2020; 47:2666-80.
- 35 Coutinho AM, Busatto GF, de Gobbi Porto FH, Faria DP, Ono CR, Garcez AT, et al. Correction to: brain PET amyloid and neurodegeneration biomarkers in the context of the 2018 NIA-AA research framework: an individual approach exploring clinical-biomarker mismatches and sociodemographic parameters. *Eur J Nucl Med Mol Imaging.* 2020;47:2715-6.
- 36 Faria DP, Duran FL, Squarzoni P, Coutinho AM, Garcez AT, Santos PP, et al. Topography of <sup>11</sup>C-Pittsburgh compound B uptake in Alzheimer's disease: a voxel-based investigation of cortical and white matter regions. *Braz J Psychiatry.* 2018;41:101-11.
- 37 McKhann GM, Knopman DS, Chertkow H, Hyman BT, Jack CR Jr, Kawas CH, et al. The diagnosis of dementia due to Alzheimer's disease: recommendations from the National Institute on Aging-Alzheimer's Association workgroups on diagnostic guidelines for Alzheimer's disease. *Alzheimer's Dement.* 2011;7:263-9.
- 38 Blessed G, Tomlinson BE, Roth M. The association between quantitative measures of dementia and of senile change in the cerebral grey matter of elderly subjects. *Br J Psychiatry.* 1968;114:797-811.
- 39 Folstein MF, Folstein SE, McHugh PR. "Mini-mental state" A practical method for grading the cognitive state of patients for the clinician. *J Psychiatr Res.* 1975;12:189-98.
- 40 Brucki SMD, Nitrini R, Caramelli P, Bertolucci PHF, Okamoto IH. [Suggestions for utilization of the mini-mental state examination in Brazil]. *Arq Neuropsiquiatr.* 2003;61:777-81.
- 41 Rodell A, Aanerud J, Braendgaard H, Gjedde A. Washout allometric reference method (WARM) for parametric analysis of [<sup>11</sup>C]PiB in human brains. *Front Aging Neurosci.* 2013;5:45.
- 42 Price JC, Klunk WE, Lopresti BJ, Lu X, Hoge JA, Ziolkowski SK, et al. Kinetic modeling of amyloid binding in humans using PET imaging and Pittsburgh compound-B. *J Cereb Blood Flow Metab.* 2005;25: 1528-47.
- 43 Smith SM, De Stefano N, Jenkinson M, Matthews PM. Normalized accurate measurement of longitudinal brain change. *J Comput Assist Tomogr.* 2001;25:466-75.
- 44 Smith SM, Zhang Y, Jenkinson M, Chen J, Matthews PM, Federico A, et al. Accurate, robust, and automated longitudinal and cross-sectional brain change analysis. *Neuroimage.* 2002;17:479-89.
- 45 Ashburner J. A fast diffeomorphic image registration algorithm. *Neuroimage.* 2007;38:95-113.
- 46 Jack CR Jr, Themeau TM, Weigand SD, Wiste HJ, Knopman DS, Vemuri P, et al. Prevalence of biologically vs clinically defined Alzheimer spectrum entities using the National Institute on Aging-Alzheimer's Association research framework. *JAMA Neurol.* 2019;76:1174-83.
- 47 Klunk WE, Koeppe RA, Price JC, Benzinger TL, Devous MD Sr, Jagust WJ, et al. The Centiloid Project: standardizing quantitative amyloid plaque estimation by PET. *Alzheimer's Dement.* 2015;11: 1-15.e1-4.
- 48 Harris PA, Taylor R, Thielke R, Payne J, Gonzalez N, Conde JG. Research electronic data capture (REDCap)—a metadata-driven methodology and workflow process for providing translational research informatics support. *J Biomed Inform.* 2009;42:377-81.
- 49 Laitinen L. Co-planar stereotaxic atlas of the human brain: 3-dimensional proportional system: an approach to cerebral imaging. By Jean Talairach and Pierre Tournoux. Translated by Mark Rayport. Georg Thieme Verlag, Stuttgart-New York, 1988. pp. 122, figs (coloured). ISBN 313711701-1 (Georg Thieme Verlag, Stuttgart; ISBN 0 86577 293 2 (Thieme Medical Publishers, Inc. New York). *Clin Neurol Neurosurg.* 1989;91:277-8.

- 50 Fjell AM, McEvoy L, Holland D, Dale AM, Walhovd KB, Alzheimer's Disease Neuroimaging Initiative. What is normal in normal aging? Effects of aging, amyloid and Alzheimer's disease on the cerebral cortex and the hippocampus. *Prog Neurobiol.* 2014;117:20-40.
- 51 Oliveira FPM, Moreira AP, de Mendonça A, Verdelho A, Xavier C, Barroca D, et al. Can 11C-PiB-PET relative delivery R1 or 11C-PiB-PET perfusion replace 18F-FDG-PET in the assessment of brain neurodegeneration? *J Alzheimers Dis.* 2018;65:89-97.
- 52 Peretti DE, Garcia DV, Reesink FE, Doorduyn J, de Jong BM, De Deyn PP, et al. Diagnostic performance of regional cerebral blood flow images derived from dynamic PIB scans in Alzheimer's disease. *EJNMMI Res.* 2019;9:59.
- 53 Peretti DE, Garcia DV, Reesink FE, van der Goot T, De Deyn PP, de Jong B, et al. Correction: Relative cerebral flow from dynamic PIB scans as an alternative for FDG scans in Alzheimer's disease PET studies. *PLoS One.* 2019;14:e0214187.
- 54 Peretti DE, Garcia DV, Reesink FE, van der Goot T, De Deyn PP, de Jong BM, et al. Relative cerebral flow from dynamic PIB scans as an alternative for FDG scans in Alzheimer's disease PET studies. *PLoS One.* 2019;14:e0211000.
- 55 Nelson PT, Alafuzoff I, Bigio EH, Bouras C, Braak H, Cairns NJ, et al. Correlation of Alzheimer disease neuropathologic changes with cognitive status: a review of the literature. *J Neuropathol Exp Neurol.* 2012;71:362-81.
- 56 Zimmer ER, Parent MJ, Souza DG, Leuzy A, Lecrux C, Kim HI, et al. [18F]FDG PET signal is driven by astroglial glutamate transport. *Nat Neurosci.* 2017;20:393-95.
- 57 Herculano-Houzel S. The glia/neuron ratio: How it varies uniformly across brain structures and species and what that means for brain physiology and evolution. *Glia.* 2014;62:1377-91.
- 58 Sojkova J, Driscoll I, Iacono D, Zhou Y, Codispoti KE, Kraut MA, et al. In vivo fibrillar  $\beta$ -amyloid detected using [11C]PiB positron emission tomography and neuropathologic assessment in older adults. *Arch Neurol.* 2011;68:232-40.
- 59 Bangen KJ, Clark AL, Edmonds EC, Evangelista ND, Werhane ML, Thomas KR, et al. Cerebral blood flow and amyloid- $\beta$  interact to affect memory performance in cognitively normal older adults. *Front Aging Neurosci.* 2017;9:181.
- 60 Greicius MD, Srivastava G, Reiss AL, Menon V. Default-mode network activity distinguishes Alzheimer's disease from healthy aging: evidence from functional MRI. *Proc Natl Acad Sci U S A.* 2004;101:4637-42.
- 61 Leech R, Sharp DJ. The role of the posterior cingulate cortex in cognition and disease. *Brain.* 2014;137:12-32.
- 62 Huang CW, Hsu SW, Chang YT, Huang SH, Huang YC, Lee CC, et al. Cerebral perfusion insufficiency and relationships with cognitive deficits in Alzheimer's disease: a multiparametric neuroimaging study. *Sci Rep.* 2018;8:1541.
- 63 Mosconi L, Tsui WH, Herholz K, Pupi A, Drzezga A, Lucignani G, et al. Multicenter standardized 18F-FDG PET diagnosis of mild cognitive impairment, Alzheimer's disease, and other dementias. *J Nucl Med.* 2008;49:390-8.
- 64 Drzezga A, Grimmer T, Henriksen G, Stangier I, Pernecky R, Diehl-Schmid J, et al. Imaging of amyloid plaques and cerebral glucose metabolism in semantic dementia and Alzheimer's disease. *Neuroimage.* 2008;39:619-33.
- 65 Lowe VJ, Lundt ES, Senjem ML, Schwarz CG, Min HK, Przybelski SA, et al. White matter reference region in PET studies of 11C-Pittsburgh compound B uptake: effects of age and amyloid- $\beta$  deposition. *J Nucl Med.* 2018;59:1583-9.
- 66 Zeydan B, Schwarz CG, Lowe VJ, Reid RI, Przybelski SA, Lesnick TG, et al. Investigation of white matter PiB uptake as a marker of white matter integrity. *Ann Clin Transl Neurol.* 2019;6:678-88.
- 67 Mattsson N, Tosun D, Insel PS, Simonson A, Jack CR Jr, Beckett LA, et al. Association of brain amyloid- $\beta$  with cerebral perfusion and structure in Alzheimer's disease and mild cognitive impairment. *Brain.* 2014;137:1550-61.
- 68 Bilgel M, Beason-Held L, An Y, Zhou Y, Wong DF, Resnick SM. Longitudinal evaluation of surrogates of regional cerebral blood flow computed from dynamic amyloid PET imaging. *J Cereb Blood Flow Metab.* 2019;40:288-97.
- 69 Ceccarini J, Bourgeois S, Van Weehaeghe D, Goffin K, Vandenberghe R, Vandembulcke M, et al. Direct prospective comparison of 18F-FDG PET and arterial spin labelling MR using simultaneous PET/MR in patients referred for diagnosis of dementia. *Eur J Nucl Med Mol Imaging.* 2020;47:2142-54.